Delft University of Technology

Adaptable digital human models from 3D body scans

Danckaers, Femke ; Huysmans, Toon; Sijbers, Jan

DOI
Publication date
2019
Document Version
Final published version
Published in
DHM and Posturography

Important note
To cite this publication, please use the final published version (if applicable).
Please check the document version above.

Chapter 33

Adaptable digital human models from 3D body scans

Femke Danckaers[1], Toon Huysmans[1,2] and Jan Sijbers[1]

[1]*imec − Vision Lab, Department of Physics, University of Antwerp, Antwerp, Belgium;* [2]*Applied Ergonomics and Design, Department of Industrial Design, CE Delft, The Netherlands*

1. Introduction

When designing wearables, realistic virtual mannequins that represent body shapes that occur in a specific target population are valuable tools for product developers. Such tools (digital human models) are already widespread (Caporaso et al., 2017, pp. 479−488; Kakizaki, Urii, & Endo, 2016; Mochimaru, 2017; Shen et al., 2017) but are often an oversampled representation of the population, based on 1D measurements. Therefore, the entire 3D shape variation is not incorporated (Blanchonette, 2010; Moes, 2010; van der Meulen & Seidl, 2007). The body shape is modified by scaling the body parts. This is not sufficient for designing products that have to fit tightly to the body (Bragança, Arezes, Carvalho, & Ashdown, 2016).

An alternative way to capture the variability of shapes in a population is to represent these shapes by statistical shape models (SSMs) (Cootes, Taylor, Cooper, & Graham, 1995; Park & Reed, 2015). Statistical shape modeling is a well-known technique in 3D anthropometric analyses to map out the variability of body shapes. It allows gaining a better understanding of the variation in shapes present in a population. SSMs are highly valuable for product designers because ergonomic products for a specific target population can be designed from these SSMs. By adapting the parameters of the SSM, a new, realistic shape can be formed. Product developers may exploit SSMs to design virtual design mannequins and explore the body shapes belonging to a percentile of a target group, for example, to visualize extreme shapes. Moreover, an SSM allows to simulate a specific 3D body shape (Park, Lumeng, Lumeng, Ebert, & Reed, 2015), which is useful for customization in a (possibly automated) workflow.

When scanning people in a standing pose, posture differences may occur over the population. If SSMs are built from these 3D scans, body posture will have a significant and often undesired influence on the shape modes. Even when the subjects are instructed to maintain a standard pose, slight posture changes are unavoidable, especially in the region of the arms. As a result, some shape variances are unintentionally correlated with posture. Posture changes are, for example, also present in the Civilian American and European Surface Anthropometry Resource (CAESAR) database (Robinette, Daanen, & Paquet, 1999). In addition, this results in a noncompact model, as posture variances lead to large deviations from the mean shape. Therefore, the computational cost when using more compact SSMs will be significantly reduced as less modes are necessary to describe the population. In this chapter, we propose a framework that has low computational complexity to build a posture-invariant SSM by capturing and correcting the posture of an instance.

2. Methods

In this section, a framework to obtain posture-invariant SSMs is described. First, an SSM is built from a population of 3D human body scans. Therefore, all 3D scans are brought into correspondence with each other. A SSM is built from those corresponded surfaces. Next, the feature modification technique is described. Finally, the posture normalization method is explained.
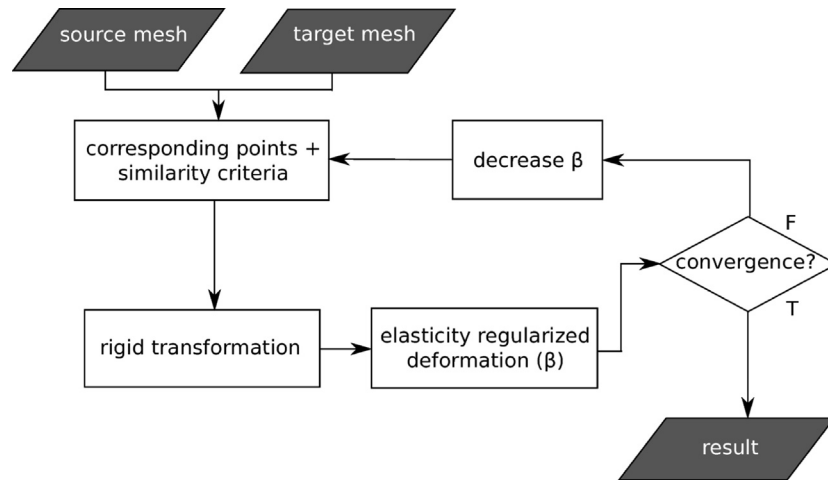
FIGURE 33.1 The surface registration framework.

2.1 Surface correspondence

In the surface registration part, the reference surface is registered to a target surface, such that the geometric distance between those surfaces becomes minimal while retaining optimal point correspondences. The approach is the same as the Rigidly initialized Nonrigid Iterative Closest Points with Translation vectors (RN-ICP-T) algorithm, which is also described in previous work of the authors (Danckaers et al., 2014). This algorithm combines a rigid registration with a nonrigid iterative closest points algorithm, where the displacement of the vertices is defined by translation vectors. In the first stage, a closest point correspondence is presumed. Throughout the iterations, the point correspondences gradually improve because of the improved geometric fit. The reference surface is uniformly resampled by the Poisson-disk sampling algorithm (Cignoni et al., 2008; Corsini, Cignoni, & Scopigno, 2012).

A global rigid registration and an elasticity-modulated registration are iteratively repeated. During the iterations, the stiffness gradually decreases, allowing the surface to become more elastic throughout the iterations to assure a robust registration algorithm. Hence, in the first iterations, a rough alignment is performed to avoid getting stuck in a local minimum, while in the last iterations, the surface will be highly elastic to ensure a perfect geometric fit. The framework is illustrated in Fig. 33.1.

In the first step of the iterative process, the surfaces are rigidly aligned. To that end, corresponding points are found using normal-ray casting from each vertex of the reference surface to the target surface. The intersection point that lies on the target surface, and is not necessarily a vertex, may be a corresponding point. A number of constraints are imposed on the corresponding points:

- The normal of the intersection has to point in the same direction (within a tolerance of 30°) as the normal of the source point.
- The distance between corresponding points has to be smaller than 20 times the average distance between the two surfaces as measured from the previous iteration. In the first iteration, the previous average distance is set to infinity.
- The casted ray may not intersect the source nor the target surface multiple times before reaching the corresponding point.

If no corresponding point is found, it has no influence on the alignment of the surfaces. Based on the corresponding points, a linear least-squares alignment is performed to determine the transformation matrix that minimizes the distance between the corresponding points.

For the elasticity-regularized deformation, the vertices are allowed to move separately while motion is restricted by a stiffness parameter β that regulates the strength of the connection with the neighboring vertices, which gradually decreases during the iterations. Hence, the movement of neighboring vertices is constrained, resulting in similar movements of neighboring vertices, as displayed in Figs. 33.2 and 33.3.

By applying weights to each vertex, the influence of this vertex can be set. If no corresponding point for a vertex of the source mesh is found, its weight is set to zero. In that case, this vertex simply moves along with its neighboring vertices.

Let n be the number of vertices of the surface and e the number of edges. The weights corresponding to the vertices are stored as elements of the diagonal matrix $W \in \mathbb{R}^{n \times n}$. Matrix $S \in \mathbb{R}^{n \times 3}$ and matrix $T \in \mathbb{R}^{n \times 3}$ hold the coordinates of the
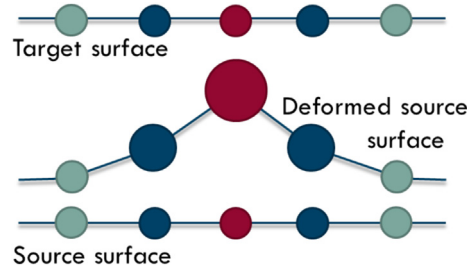
FIGURE 33.2 Schematic representation of elasticity. If one vertex, in this case, the *red dot* (gray in print version) is transformed; the neighboring vertices are forced to move along with this vertex. The closest neighbors (*blue dots*) (dark gray in print version) are the stiffest and move more than the distant neighbors (*green dots*) (light gray in print version).
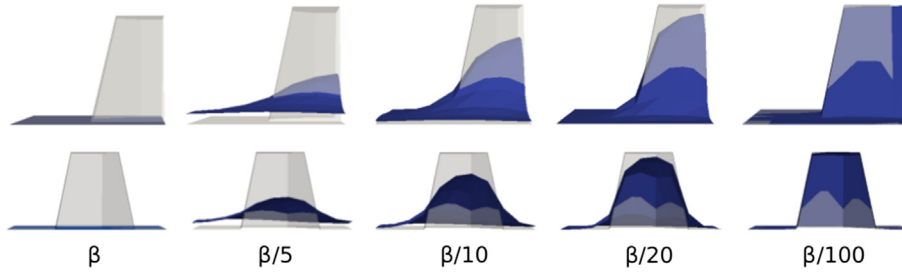
FIGURE 33.3 Influence of the elasticity parameter on the elastic surface deformation, shown from two viewpoints. In each figure, the target surface is visualized in transparent white and the deformed source in blue (black in print version). The left example is created with a very high stiffness factor. The right example is created with a very low stiffness factor. From left to right, the stiffness factor decreases.

corresponding source and target vertices, respectively. Matrix $0 \in \mathbb{R}^{e \times 3}$ is a matrix that contains only zeros. The optimal translation vectors, the matrix $X_t \in \mathbb{R}^{n \times 3}$, are found by solving the following linear system:

$$\begin{bmatrix} \beta C \\ WI \end{bmatrix} X_t = \begin{bmatrix} 0 \\ W(T - S) \end{bmatrix},$$

with $C \in \mathbb{R}^{e \times n}$ being the incidence matrix of the reference surface that indicates the start and end vertex of each edge. The rigid registration step and elastic registration steps are iteratively repeated until convergence is reached, which is calculated by comparing the current distance between the source and reference surface d_t and the previous distance between the source and reference surface d_{t-1}. In our case, convergence was reached if

$$\frac{|d_t - d_{t-1}|}{d_t} < 0.001.$$

2.2 Building a statistical shape model

An SSM is built from a population of N shapes, with every shape consisting of n vertices. As such, the population is represented by a $3n$-dimensional point cloud, where each point represents a shape. Using principal components analysis, this cloud can be represented by a mean shape and $N-1$ eigenmode vectors, where the first eigenmode describes the largest variance in the population, the second eigenmode the second largest variance perpendicular to the first, and so forth (Cootes et al., 1995). The framework is shown in Fig. 33.4.

In an SSM, the mean shape $\bar{x} \in \mathbb{R}^{3n}$ and the main shape modes, or the principal component (PC) modes of the shape model $P \in \mathbb{R}^{3 \times (N-1)}$, are incorporated. This means that a new shape $y \in \mathbb{R}^{3n}$ that lies within the shape space of the model can be formed by adding a linear combination of the PCs to the mean shape:

$$y = \bar{x} + Pb,$$

with $b \in \mathbb{R}^{N-1}$ being the vector containing the SSM parameters.
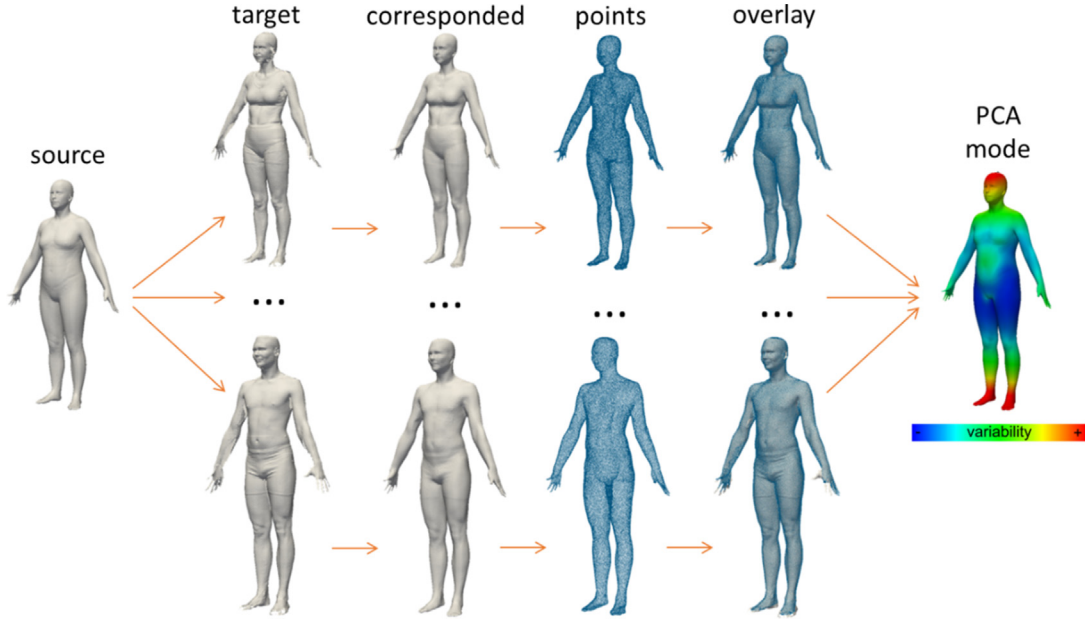
FIGURE 33.4 Framework for building a statistical shape model. First, a source surface is registered to each surface of the population. From these registered surfaces, a statistical shape model is built. *PCA*, principal components analysis.

2.3 Feature modification

A specific feature of an individual's shape, such as height, can be adapted by adding a linear combination of PCs to the individual's shape vector. The weights for this linear combination, the so-called feature vector, are computed via multiple linear regression of the PC weights on the body features for the population of individuals. By applying a scaled version of the feature vector to the shape vector of an individual, its shape can be adapted to match a specific feature value (Danckaers, Huysmans, Lacko, & Sijbers, 2015).

Suppose we know F features $\boldsymbol{f}_i = [f_1 \ f_2 \ f_3 \ \cdots \ f_F \ 1]^T \in \mathbb{R}^{F+1}$ and the PC weights $\boldsymbol{b}_i \in \mathbb{R}^{N-1}$ of each shape i from the data set, then a mapping matrix $M \in \mathbb{R}^{(N-1) \times (F+1)}$ describing the relationship between the PC weights matrix $\boldsymbol{B} = [\boldsymbol{b}_1 \ \boldsymbol{b}_2 \ \boldsymbol{b}_3 \ \cdots \ \boldsymbol{b}_N] \in \mathbb{R}^{(N-1) \times N}$ and the feature matrix $\boldsymbol{F} = [\boldsymbol{f}_1 \ \boldsymbol{f}_2 \ \boldsymbol{f}_3 \ \cdots \ \boldsymbol{f}_N] \in \mathbb{R}^{(F+1) \times N}$ is calculated by

$$M = BF^+,$$

where $\boldsymbol{F}^+$ is the pseudoinverse of $\boldsymbol{F}$.

With this mapping matrix, new PC weights $\boldsymbol{b}$ can be generated from given features $\boldsymbol{f}$ by

$$b = Mf.$$

2.4 Identity removal

By removing the identity of each body scan, shape-specific deformations are filtered out, and only posture-related deformations remain. To do so, the features of each shape are adjusted so that they are equal to the features of the average shape of the data set. As a result, all shapes look similar.

First, the specific PC weight vector $\boldsymbol{b}_i$ of instance i is extracted from the PC matrix $\boldsymbol{B}$. Second, the delta feature vector $\Delta \boldsymbol{f}$, which is the vector that holds the values that should be added to the current features to become equal to the average features, is calculated by extracting the specific features $\boldsymbol{f}_i$ (defined as the ith column of $\boldsymbol{F}$) of instance i from the average features $\bar{\boldsymbol{f}}$ of the population:

$$\Delta f = \bar{f} - f_i.$$

Next, the delta PC weights vector $\Delta \boldsymbol{b}$, which should be added to the current PC weights to adjust the body shape, is calculated by multiplying the mapping matrix $\boldsymbol{M}$ with the calculated delta features $\Delta \boldsymbol{f}$:

$$\Delta b = M \cdot \Delta f \cdot$$

These delta weights are subsequently added to the original PC weights $\boldsymbol{b}_i$ to obtain the PC weights $\boldsymbol{b}_i'$ of the shape with average features:

$$b_i' - b_i + \Delta b.$$

Finally, new shapes without identity, x_i', are calculated by multiplying the new weights b_i' with the PC vectors P_s of the SSM and adding them to the mean shape $\bar{x}$:

$$x_i' = \bar{x} + P_s b_i'.$$

From the set of shapes without identity, a new SSM is built (F. Danckaers et al., 2014), which represents a posture model. The result is a posture model whose variances are mainly the posture variances.

2.5 Posture normalization

To normalize the posture of a shape, that shape is corresponded with the statistical posture model by elastic surface registration (Danckaers et al., 2014). Note that the posture model and the new shape do not have to stem from the same data set. It is sufficient that they have roughly the same pose. From the corresponded posture model, the PC weights are calculated. Because this model mostly contains posture variations, only the posture of the target shape is captured.

First, the input shape, x, is scaled, such that it has the same height as the posture model. Then, the posture PC weights b_i of x_i are calculated by multiplying the inverse of PC matrix P_p of the posture model by the distance vector between each vertex of the input surface mesh and the mean surface mesh $\bar{x}$. These posture PC weights only denote differences in posture compared with the mean posture.

$$b_i = P_p^T (x_i - \bar{x}).$$

Next, the posture x_i' of the input shape is reconstructed from the calculated posture PC weights b_i:

$$x_i' = \bar{x} + P_p b_i.$$

Finally, the normalized shape $\hat{x}$ is calculated by subtracting the posture influence $P_p b_i$ on the shape from the original shape x_i:

$$\hat{x}_i = x_i - P_p b_i.$$

3. Results

To validate the algorithms, we used scans from the Dutch CAESAR database (Robinette et al., 1999). This is an extensive database that contains 3D scans, measurements, and other meta-data of over 1000 people in standing pose. All subjects were scanned using the Vitronic Vitus Pro laser scanner (Vitronic, 1995).

In the following subsections, an SSM in standing pose is built, and the different steps to construct a posture-normalized SSM are illustrated. Moreover, shape prediction from a set of features is illustrated.

3.1 Statistical shape model

An SSM was built from 700 subjects (350 men and 350 women) in standing pose from the CAESAR database (Robinette et al., 1999). The 3D scans were registered using the same template surface mesh, a digitally modeled body consisting of 100k uniformly distributed vertices (Valette, Chassery, & Prost, 2008). No posture changes were made to these meshes yet. In Fig. 33.5, the first three PC modes of the SSM built from the original shapes are shown. Influence of posture is visible in the third mode.

3.2 Posture-normalized shape model

In Fig. 33.6, two examples of identity removal are shown. The resulting shapes look more similar than the original shapes. The features that were used for identity removal are gender, acromial height sitting, ankle circumference, spine-to-shoulder length, spine-to-elbow length, arm length (spine to wrist), arm length (shoulder to wrist), arm length (shoulder to elbow), armscye circumference (scye circumference over acromion), bizygomatic breadth, chest circumference, bust/chest circumference under bust, buttock-knee length, chest girth (chest circumference at scye), crotch height, elbow height sitting, eye height sitting, face length, foot length, hand circumference, hand length, head breadth, head circumference, head length, hip breadth sitting, hip circumference maximum, hip circ max height, knee height, neck base circumference, shoulder breadth, sitting height, stature, subscapular skinfold, thigh circumference, thigh circumference max sitting, thumb tip reach (TTR 1, TTR 2, TTR 3), triceps skinfold, crotch length, vertical trunk circumference, waist circumference preferred, waist front length, waist height preferred, and weight. The posture model is shown in Fig. 33.7. It was cut off at 12 shape modes to reduce shape-related variations and remove noise from higher modes. This number was empirically determined by manually inspecting the shape modes.
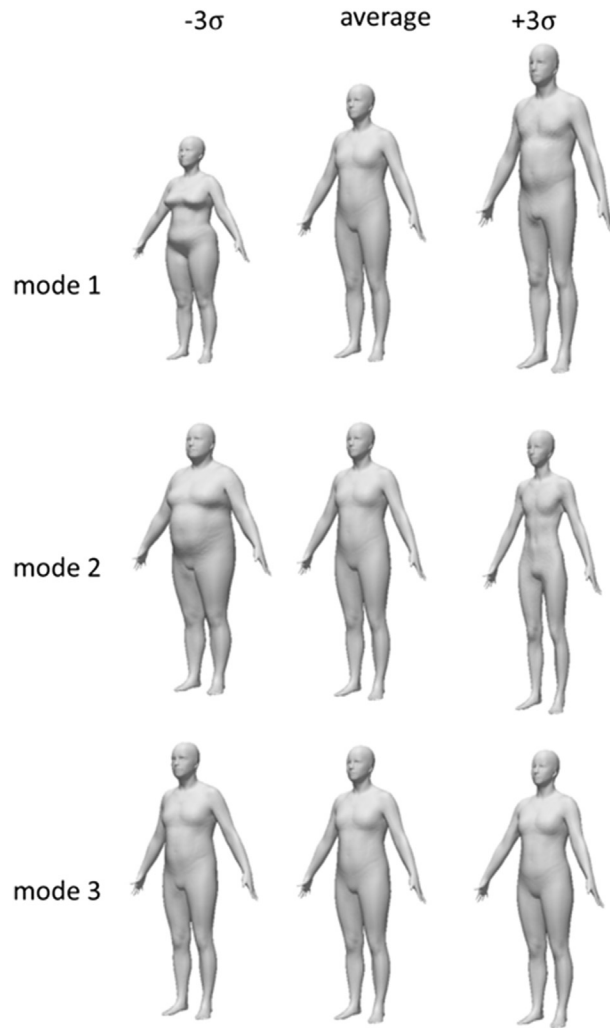
FIGURE 33.5 The first three eigenmodes of the nonnormalized SSM, built from the original shapes. A posture variation is clearly noticeable in the third mode, where the position of the arms and shoulders differs. *SSM*, statistical shape model.
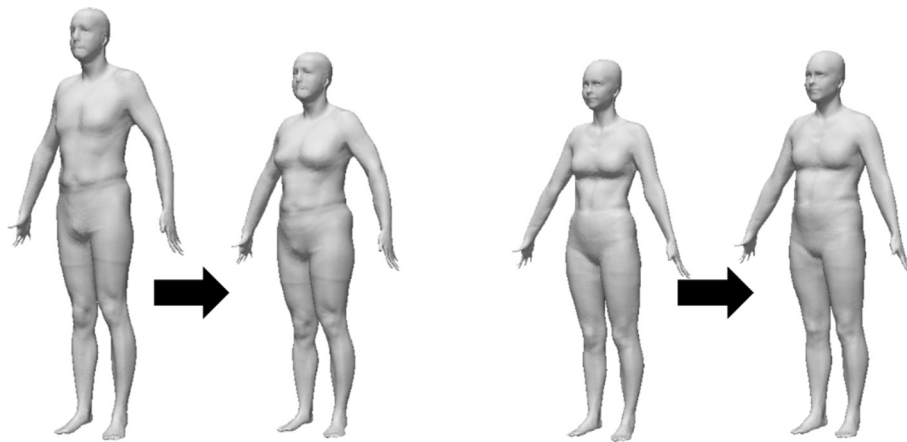
FIGURE 33.6 Two examples of identity removal.
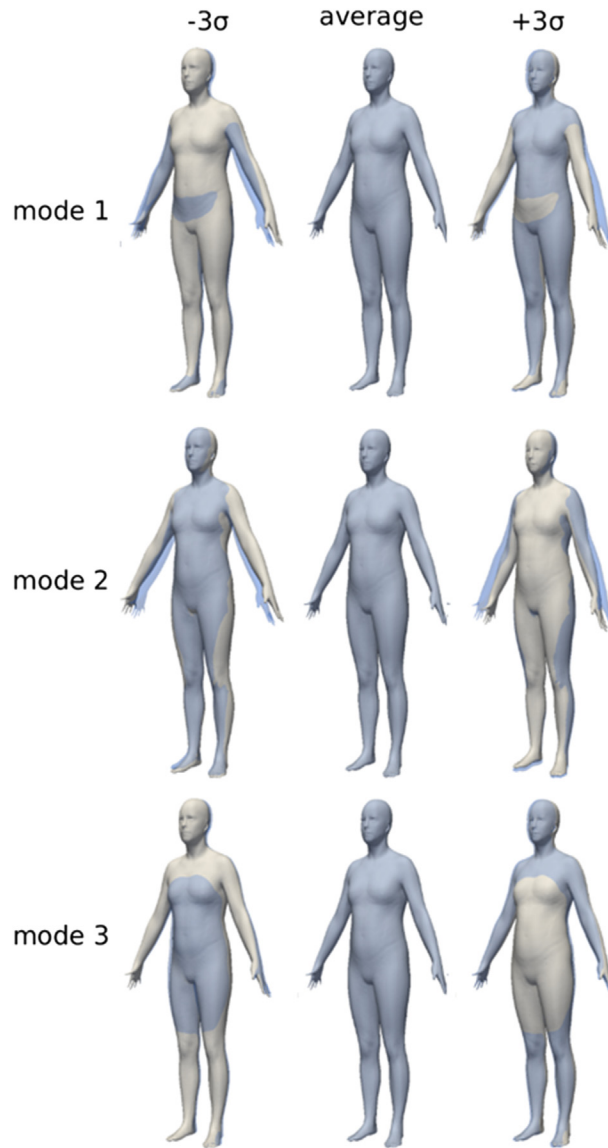
FIGURE 33.7   The first three eigenmodes of the posture model. Posture variation is mainly visible in the region of the arms and torso. For every shape, the average shape is overlaid in blue (dark gray in print version) to show the difference in posture more clearly.

Then, the posture of every input shape of the original SSM was corrected. These shapes served as input to build a new, posture-normalized SSM. The first three shape modes of this posture-normalized SSM are shown in Fig. 33.8.

3.3 Model performance—compactness

Compactness is a widely used measure for quantifying the correspondence quality of an SSM (Davies, Twining, Cootes, Waterton, & Taylor, 2002; Su, 2011). A compact SSM is a model that has as little variance as possible and requires as few parameters as possible to define an instance. This suggests that the important information is captured in a plot of cumulative variance. Therefore, calculation time decreases significantly when using the SSM for shape prediction from parameters (Danckaers et al., 2015). The compactness $C(m)$ is expressed as the sum of variances of the SSM using m shape modes,

$$C(m) = \sum_{i=1}^{m} \lambda_i,$$

where λ_i is the variance in mode i.

Fig. 33.9 shows the compactness as a function of the number of shape modes. The normalized SSM is more compact than the nonnormalized SSM. For example, to describe more than 90% of the shape variation inside the population, the
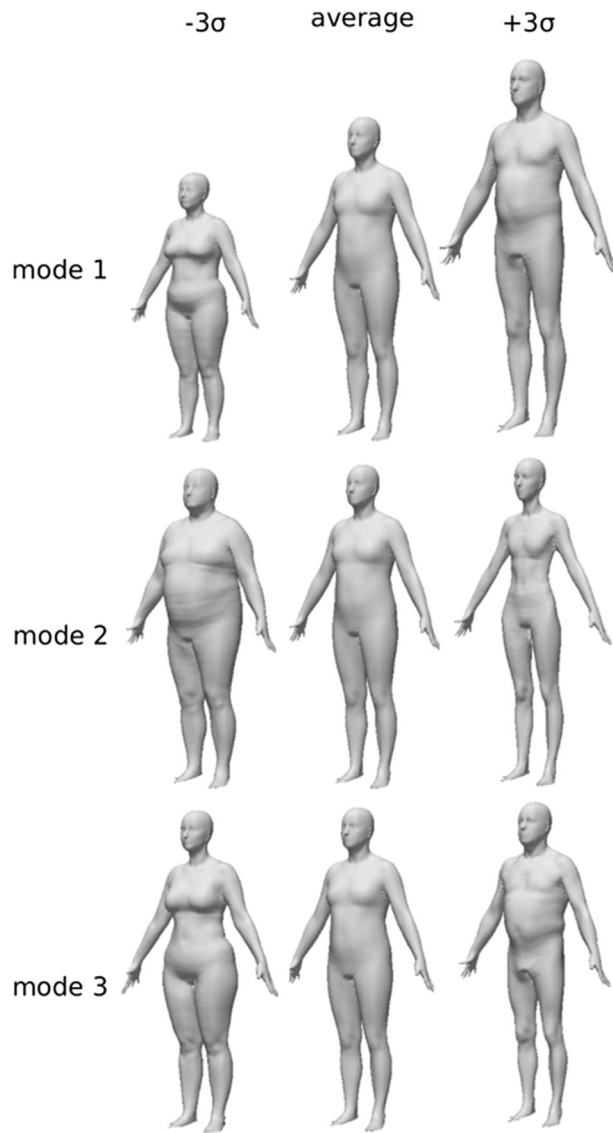
FIGURE 33.8 First three eigenmodes of the posture-normalized SSM. The modes describe body shape variances better than the shape modes of the nonnormalized SSM, as shown in Figure 5. Note that the third mode of the normalized SSM describes mainly gender, while the third mode of the nonnormalized SSM describes mainly the position of the arms. *SSM*, statistical shape model.
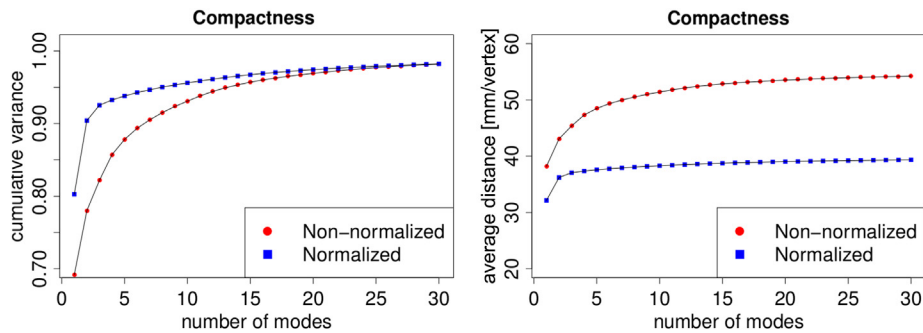
FIGURE 33.9 Compactness graphs, with only the first 30 shape modes plotted. The average deviation from the mean shape of a shape described by a specific number of shape modes. In the left figure, the cumulative variance is plotted, while in the right figure, the average deviation in mm/vertex is shown.
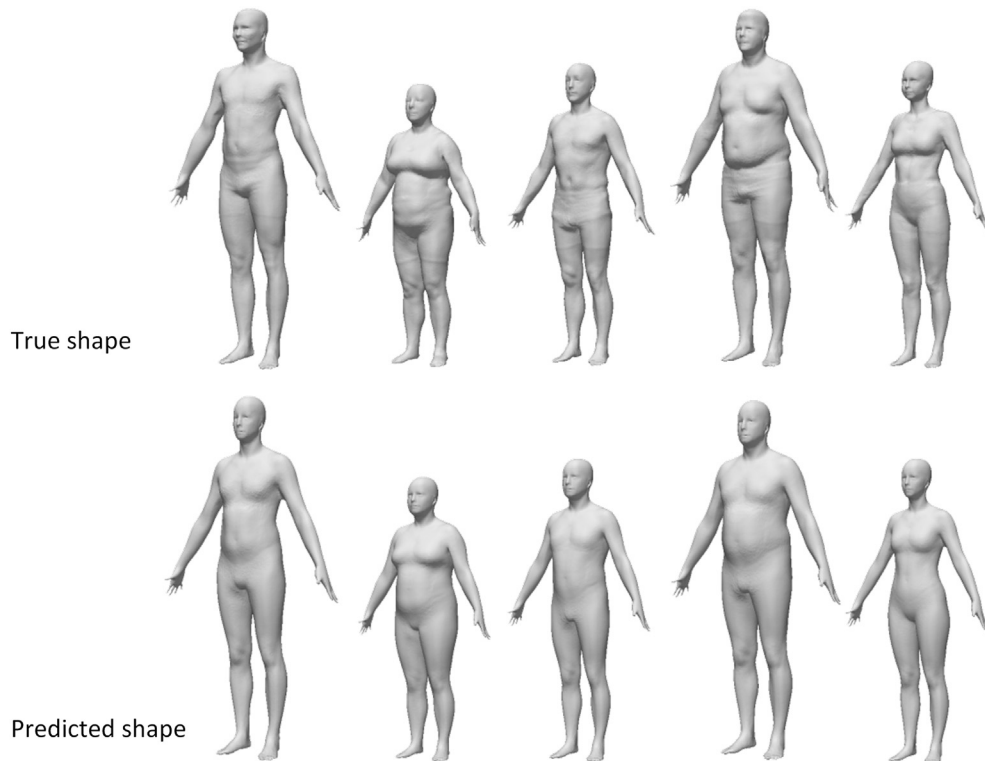
FIGURE 33.10 Examples of predicted body shapes.

nonnormalized SSM requires seven shape modes, whereas only two shape modes were sufficient for the normalized SSM. Using only one shape mode, the normalized SSM is 16% more compact than the nonnormalized SSM. For five shape modes, an improvement of 23% was observed, and an improvement of 25% using 10 shape modes. The normalized SSM is substantially more compact than the nonnormalized SSM, and more of its variance is captured in the first mode than in the nonnormalized SSM.

3.4 Shape prediction from features

An SSM is a mathematical model that can be controlled by parameters. These parameters do not necessarily have a physical meaning. A more intuitive way of adjusting a body shape is linking those parameters to physical features, such as height, weight, gender, and so forth, so the body shape is adaptable by changing the feature values. It is important to know which features influence body shape to generate an accurate posture model. An optimal set of features to predict a body shape was selected by cross-validation. The importance of each feature for predicting a body shape was determined by simulating a body shape based on features and comparing this shape with the real shape. The CAESAR database contains a lot of meta-data that do not necessarily influence the body shape. In this chapter, for posture normalization, we used all available data. Missing meta-data in the CAESAR database were estimated through imputation (Wold, 1973).

The test was applied to 20 nonnormalized shapes (10 men and 10 women) for the 14 easiest-to-measure features, using only a balance and a tape measure: gender (G), age (A), arm length (AL), breast circumference (BC), chest circumference (CC), crotch height (CH), hip circumference (HC), knee height (KH), shoulder breadth (SB), sitting height (SH), stature (S), thigh circumference (TC), waist circumference (WC), and weight (W). For every test subject, the body shape was predicted from every possible combination of its features. In Fig. 33.10, some predicted body shapes are shown. The average distance per vertex from the predicted body shape to the true body shape is calculated and visualized in Fig. 33.11. Our tests have shown that we could predict a body shape using the posture-normalized SSM, with an average error of 6.59 ± 1.28 *mm*. The largest errors appeared in the hands, feet, and stomach region. The method is also useful to visualize feature percentiles. In Fig. 33.12, we show some body shapes simulated from one given feature.
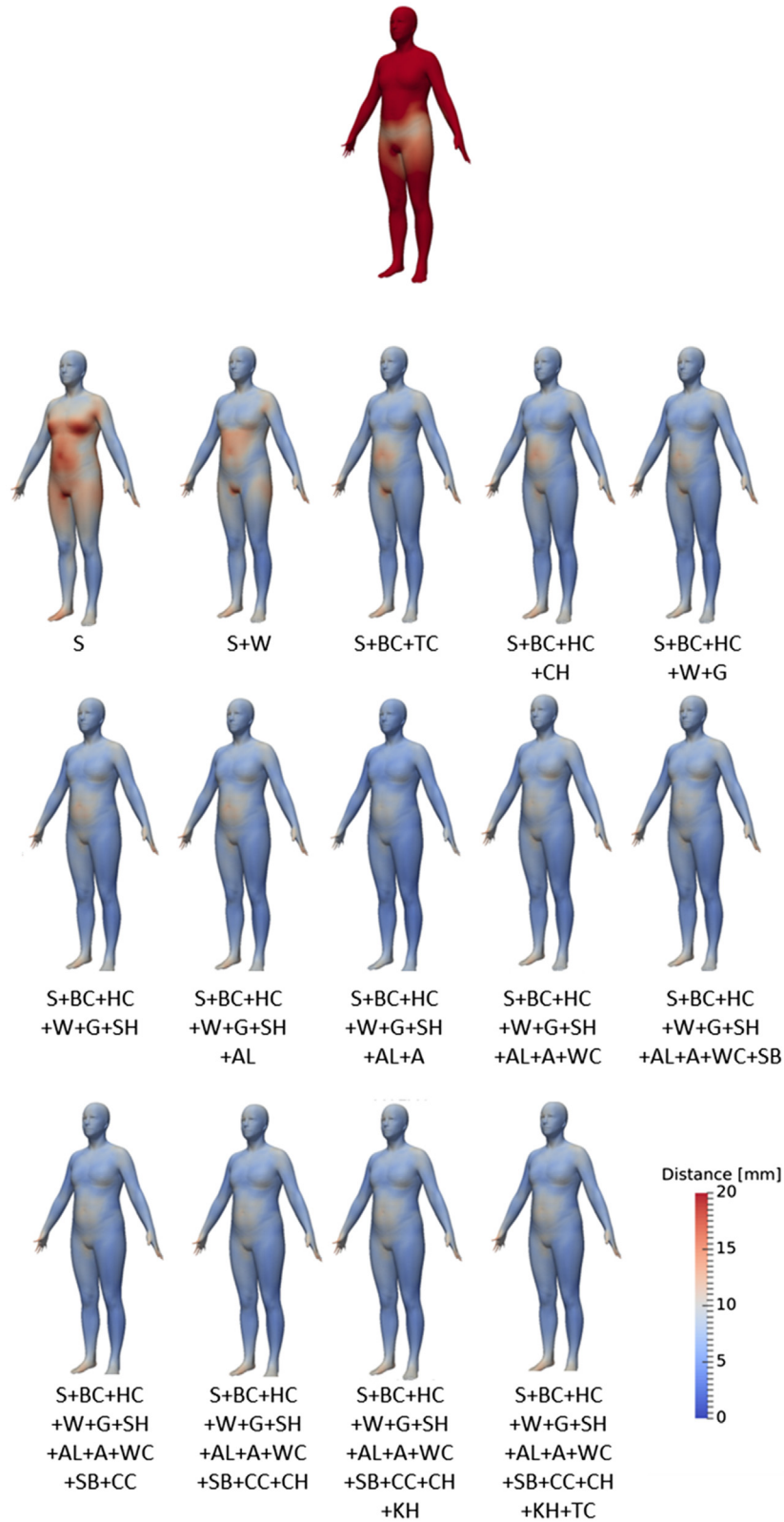
FIGURE 33.11 Colormap that denotes the average distance between the shape predicted from a set of features and true shape, in mm/vertex. The largest errors appear in the stomach region. *A*, age; *AL*, arm length; *BC*, breast circumference; *CC*, chest circumference; *CH*, crotch height; *G*, gender; *HC*, hip circumference; *KH*, knee height; *S*, stature; *SB*, shoulder breadth; *SH*, sitting height; *TC*, thigh circumference; *W*, weight; *WC*, waist circumference.
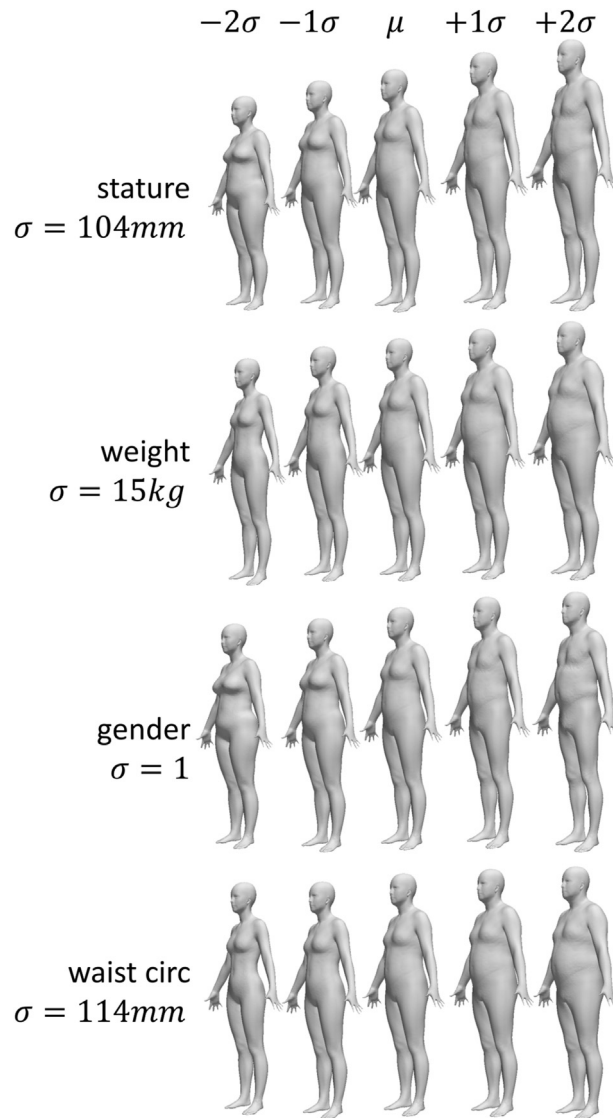
FIGURE 33.12   The most plausible body shapes from one given feature. The standard deviation σ of the feature is calculated, and the body shape is simulated for -2σ, -1σ, the average body shape μ, $+1\sigma$, and $+2\sigma$.

4. Conclusion

In this chapter, we proposed a technique to perform statistical shape analysis in a posture-invariant way. It allows us to study the shape variations in a database of human body shapes in slightly varying postures. The posture model can be used to normalize any shape that is brought into correspondence with this model in a fast and precise way.

The results have shown that statistical shape analysis of a posture-normalized population results in more shape-related variations than performing the same analysis on a nonnormalized population. The normalized SSM is a more compact representation of the population than the nonnormalized shape SSM. Hence, less shape modes are needed to describe a certain percentage of the population.

Our SSM is a valuable tool for product designers for creating more realistic, virtual mannequins, which can be used to improve the ergonomics of their products. It is also a first step toward posture-invariant statistical shape analysis of body shapes in varying poses, e.g., for predicting the body shape in seated pose from a body shape in standing pose. Therefore, one scan is sufficient for product developers to design products that require simulating the body shape in different poses.

References

Blanchonette, P. (2010). *Jack human modelling tool: A review*.

Bragança, S., Arezes, P., Carvalho, M., & Ashdown, S. (2016). Effects of different body postures on anthropometric measures. In *Advances in ergonomics in design: Proceedings of the AHFE 2016 international conference on ergonomics in design, July 27−31, 2016* (Vol. 485, pp. 313−322). Florida, USA: Walt Disney World®.

Caporaso, T., Di Gironimo, G., Tarallo, A., De Martino, G., Di Ludovico, M., & Lanzotti, A. (2017). *Digital human models for gait analysis: Experimental validation of static force analysis tools under dynamic conditions*. Cham: Springer.

Cignoni, P., Callieri, M., Corsini, M., Dellepiane, M., Ganovelli, F., & Ranzuglia, G. (2008). MeshLab: An open-source mesh processing tool. In *Eurographics Italian chapter conference*. The Eurographics Association.

Cootes, T. F., Taylor, C. J., Cooper, D. H., & Graham, J. (1995). Active shape models-their training and application. *Computer Vision and Image Understanding, 61*(1), 38−59.

Corsini, M., Cignoni, P., & Scopigno, R. (2012). Efficient and flexible sampling with blue noise properties of triangular meshes. *IEEE Transactions on Visualization and Computer Graphics, 18*(6), 914−924.

Danckaers, F., Huysmans, T., Lacko, D., Ledda, A., Verwulgent, S., Dongen, S. Van, & Sijbers, J. (2014). Correspondence preserving elastic surface registration with shape model prior. In *2014 22nd international conference on pattern recognition* (pp. 2143−2148). IEEE.

Danckaers, F., Huysmans, T., Lacko, D., & Sijbers, J. (2015). Evaluation of 3D body shape predictions based on features. In *Proceedings of the 6th international conference on 3D body scanning technologies, Lugano, Switzerland, 27−28 October 2015* (pp. 258−265). Ascona, Switzerland: Hometrica Consulting.

Davies, R. H., Twining, C. J., Cootes, T. F., Waterton, J. C., & Taylor, C. J. (2002). A minimum description length approach to statistical shape modeling. *IEEE Transactions on Medical Imaging, 21*(5), 525−537.

Kakizaki, T., Urii, J., & Endo, M. (2016). Application of digital human models to physiotherapy training. In *18th international conference on advanced vehicle technologies; 13th international conference on design education; 9th frontiers in biomedical devices* (Vol. 3)ASME.

van der Meulen, P., & Seidl, A. (2007). Ramsis - the leading cad tool for ergonomic analysis of vehicles. *Lecture Notes in Computer Science, 4561*, 1008−1017.

Mochimaru, M. (2017). Digital human models for human-centered design. *Journal of Robotics and Mechatronics, 29*(5), 783−789.

Moes, N. C. C. M. (2010). Digital human models: An overview of development and applications in product and workplace design. In *8th international symposium on tools and methods of competitive engineering (TMCE)* (pp. 73−84).

Park, B. K., Lumeng, J. C., Lumeng, C. N., Ebert, S. M., & Reed, M. P. (2015). Child body shape measurement using depth cameras and a statistical body shape model. *Ergonomics, 58*(2), 301−309.

Park, B. K., & Reed, M. P. (2015). Parametric body shape model of standing children aged 3-11 years. *Ergonomics, 58*(10), 1714−1725.

Robinette, K. M., Daanen, H. A. M., & Paquet, E. (1999). The CAESAR project: A 3-D surface anthropometry survey. In *second international conference on 3-D digital imaging and modeling* (pp. 380−386). IEEE Comput. Soc. Cat. No.PR00062.

Shen, Z., Wu, C., Ding, B., Yuan, Z., Zhang, N., Zhao, M., & Zhao, Y. (2017). GPU-based interactive near-regular texture synthesis for digital human models. *Technology and Health Care, 25*(S1), 357−365.

Su, Z. (2011). *Statistical shape Modelling : Automatic shape model building*. University College London.

Valette, S., Chassery, J. M., & Prost, R. (2008). Generic remeshing of 3D triangular meshes with metric-dependent discrete voronoi diagrams. *IEEE Transactions on Visualization and Computer Graphics, 14*(2), 369−381.

Vitronic. (1995). *Inhalte Lightbox - VITRONIC - the machine vision people*. Retrieved March 22, 2018, from https://www.vitronic.com/3d-body-scanner/3d-scan-for-3d-printing/vitus-bodyscan-benefits-3d-printing/inhalte-lightbox.html.

Wold, H. (1973). Nonlinear iterative partial least squares (NIPALS) modelling: Some current developments. In *Multivariate analysis-III* (pp. 383−407). Elsevier.